Electronic Supplementary Material (ESI) for Materials Chemistry Frontiers.

Efficient Narrowband Green OLED with TADF Sensitizers Combining Multiple Charge-Transfer Pathways

Deli Li, Jiaji Yang, Jiting Chen, Xiaomei Peng, Wei Li, Zijian Chen, Weidong Qiu, Guo-Xi Yang, Zhihai Yang, Mengke Li, Simin Jiang, Denghui Liu, Yiyang Gan, Kunkun Liu and Shi-Jian Su*

State Key Laboratory of Luminescent Materials and Devices, Institute of Polymer Optoelectronic Materials and Devices, South China University of Technology, Wushan Road 381, Guangzhou 510640, P. R. China.

E-mail: mssjsu@scut.edu.cn.

1. General Information

All reagents and solvents were purchased from commercial sources and used without further purification. ^{1}H and ^{13}C NMR spectra were recorded on a Bruker NMR spectrometer. Matrix-assisted laser desorption/ionization-time of flight (MALDI-TOF) mass spectrum was recorded using an AXIMACFRTM plus instrument. UV-vis absorption spectra were recorded using Perkin-Elmer Lambda 950-PKA UV-Vis. Both room temperature and 77 K fluorescence and phosphorescent spectra were recorded by FluoroMax-4 spectrofluorometer (Horiba Jobin Yvon). The phosphorescent spectra were measured with a delay time of 5 ms. Cyclic voltammograms of the investigated compounds were measured with 0.1 M n-Bu_4NPF_6 dissolved in anhydrous CH_2Cl_2/CH_2CN (4:1 volume ratio) through the three-electrode system of the CHI-600D electrochemical workstation at a scanning rate of 100 mV s^{-1}. Photoluminescence quantum yields (PLQYs) of films were measured utilizing an integrating sphere of Hamamatsu absolute PLQY spectrometer (C11347-01). Transient PL decay and time-resolved emission spectra were investigated under N_2 atmosphere using Quantaurus-Tau fluorescence lifetime measurement system with 371 nm LED excitation source (C11367-03, Hamamatsu Photonics Co., Japan).

2. Synthesis of Materials

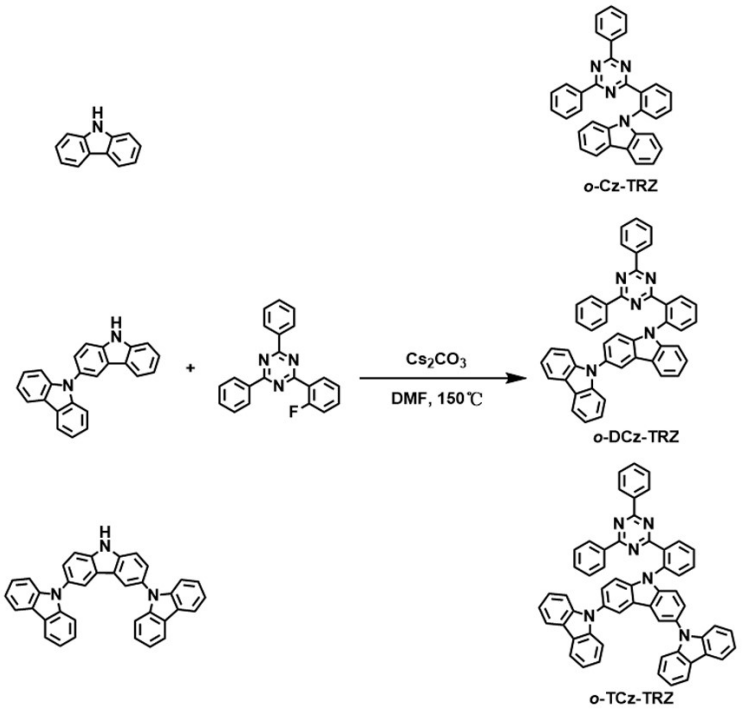

Scheme S1. Synthetic routes of the investigated compounds.

The target product *o*-Cz-TRZ was synthesized according to the reported literatures.[1,2] All compounds were easily purified by column chromatography and train sublimation. Chemical structures of all compounds were fully characterized by ^{1}H and ^{13}C NMR and matrix-assisted laser desorption/ionization-time of flight (MALDI-TOF) mass spectrum.

9-(2-(4,6-diphenyl-1,3,5-triazin-2-yl) phenyl)-9*H*-3,9'-bicarbazole (*o*-DCz-TRZ):

2-(2-Fluorophenyl)-4,6-diphenyl-1,3,5-triazine (1 g, 3 mmol), 9*H*-3,9'-bicarbazole (1 g, 3 mmol) and cesium carbonate (1.95 g, 6 mmol) were added into a three-neck flask in 100 mL *N, N*-dimethylformamide in N_2 atmosphere. After degassing for 30 min, the mixture was stirred and refluxed overnight. After removing the solvent in vacuum, the mixture was partitioned between DCM and water. The combined organic layers were washed with brine, dried over $MgSO_4$ and concentrated in vacuo. Column chromatography of the residue solid (eluent: DCM/ PE = 1/2) afforded 1.5 g yellow-green solid. Yield: 78%.

^{1}H NMR (400 MHz, DMSO) δ 8.62 (dd, *J* = 7.8, 1.3 Hz, 1H), 8.27 (d, *J* = 1.9 Hz, 1H), 8.22 (d, *J* = 7.8 Hz, 3H), 8.08 – 7.98 (m, 6H), 7.92 (td, *J* = 12, 1.6 Hz, 1H), 7.57 (t, *J* = 7.4 Hz,

2H), 7.47 – 7.36 (m, 6H), 7.36 – 7.16 (m, 9H). ^{13}C NMR (126 MHz, $CDCl_3$) δ 172.02, 171.28, 142.40, 141.71, 140.53, 136.49, 135.62, 135.35, 132.91, 132.65, 132.48, 130.35, 129.37, 128.96, 128.75, 128.38, 126.73, 125.75, 125.21, 124.54, 123.18, 122.98, 120.48, 120.15, 120.11, 119.45, 119.22, 110.52, 110.03, 109.79. MALDI-TOF: calcd for $C_{45}H_{29}N_5$, 639.7620; found, 640.1564.

9'-(2-(4,6-diphenyl-1,3,5-triazin-2-yl) phenyl)-9'*H*-9,3':6',9''-tercarbazole (*o*-TCz-TRZ): 2-(2-Fluorophenyl)-4,6-diphenyl-1,3,5-triazine (1 g, 3 mmol), 9*H*-3,9'-bicarbazole (1.5 g, 3 mmol) and cesium carbonate (1.95 g, 6 mmol) were added into a three-neck flask in 100 mL *N, N*-dimethylformamide in N_2 atmosphere. After degassing for 30 min, the mixture was stirred and refluxed overnight. After removing the solvent in vacuum, the mixture was partitioned between DCM and water. The combined organic layers were washed with brine, dried over Mg_2SO_4 and concentrated in vacuo. Column chromatography of the residue solid (eluent: DCM/ PE= 1/1) afforded 1.8 g yellow-green solid. Yield: 75%.
^{1}H NMR (400 MHz, CD_2Cl_2) δ 8.79 – 8.67 (m, 1H), 8.28 – 8.18 (m, 4H), 8.16 – 8.07 (m, 6H), 7.98 – 7.92 (m, 2H), 7.89 – 7.77 (m, 1H), 7.53 – 7.44 (m, 6H), 7.43 – 7.28 (m, 9H), 7.27 – 6.95 (m, 7H). ^{13}C NMR (101 MHz, CD_2Cl_2) δ 173.41, 172.60, 142.98, 142.56, 137.45, 136.69, 136.45, 134.33, 134.26, 133.97, 131.50, 131.22, 130.51, 129.99, 129.77, 127.27, 127.15, 125.57, 124.28, 121.40, 120.88, 120.78, 112.45, 110.96. MALDI-TOF: calcd for $C_{57}H_{36}N_6$, 804.9570; found, 805.4374.

3. Thermal Properties

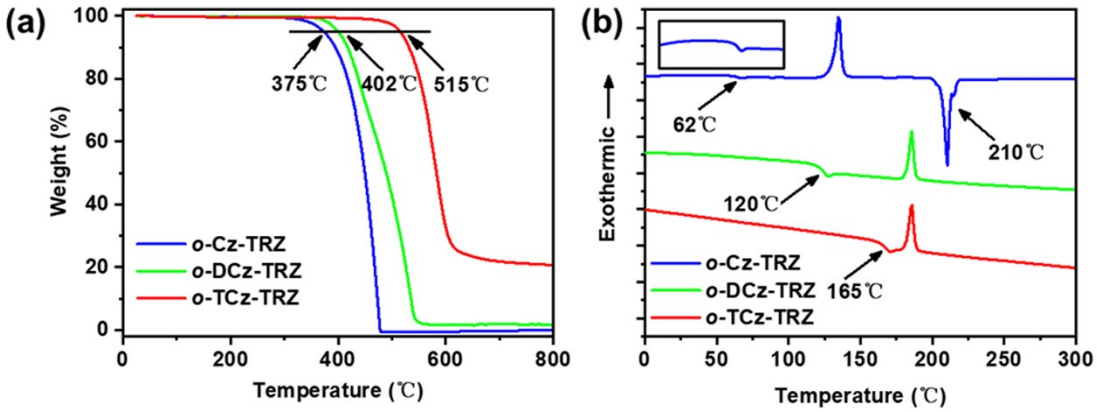

Fig. S1 (a) Thermogravimetric analysis (TGA) curves and (b) differential scanning calorimetry (DSC) curves of *o*-Cz-TRZ, *o*-DCz-TRZ and *o*-TCz-TRZ.

4. Cyclic Voltammetry

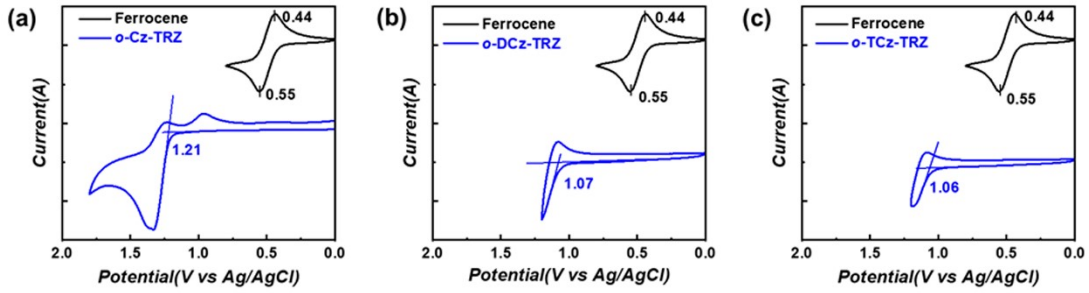

Fig. S2 Cyclic voltammograms of (a) *o*-Cz-TRZ, (b) *o*-DCz-TRZ and (c) *o*-TCz-TRZ.

Solid state ionization potential (IP) is estimated by the onset potential of redox peak as shown in Figure S2 and calculated according to the formula S1,[3] where 4.8 eV is the formal potential of ferrocenium/ferrocene (Fc+/Fc) redox couple at vacuum level. The IPs of *o*-Cz-TRZ, *o*-DCz-TRZ and *o*-TCz-TRZ are -5.52, -5.38 and -5.37 eV, respectively.

E_{HOMO}= IP = - [E_{ox} - E_{ox} (Fc/Fc+) + 4.8] eV (S1)

5. Quantum Chemical Computation

All of the simulations were performed using the Gaussian 09_B01 program package. For all the investigated molecules, the ground state geometries and electron distributions were optimized at B3LYP/6-31G** level in vacuum. Based on the optimized geometries, the characteristics of excited states were optimized at the B3LYP/6-31G** level. RDG isosurfaces and scattering diagrams analyses were performed based on the wavefunction information of the investigated molecules in virtue of Multiwfn and VMD software.[4-6]

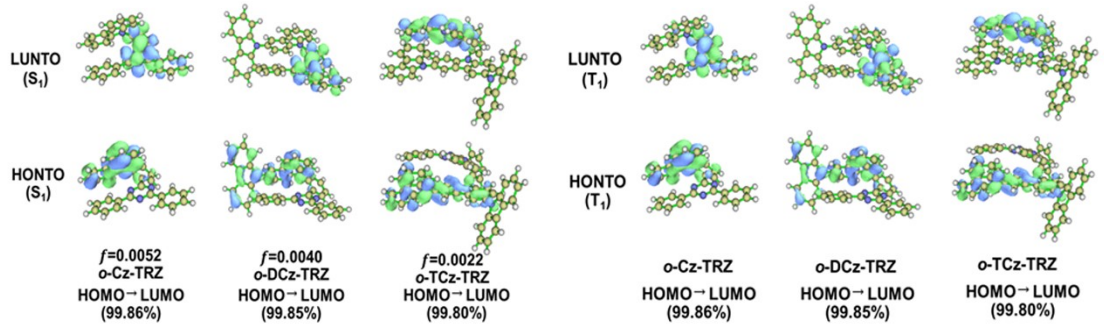

Fig. S3 NTO analysis of S_1 and T_1 states and oscillator strength (f) of S_1 based on B3LYP/6-31G**.

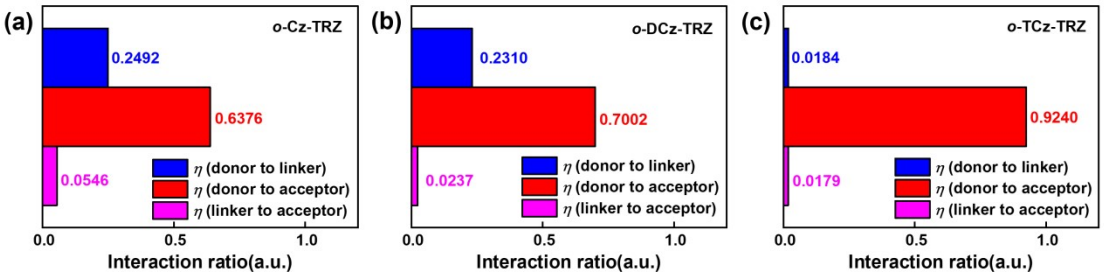

Fig. S4 The contribution ratio (η) for the electron transition from donor to linker, donor to acceptor and linker to acceptor at the S_1 excited state.

6. Photoluminescence Properties

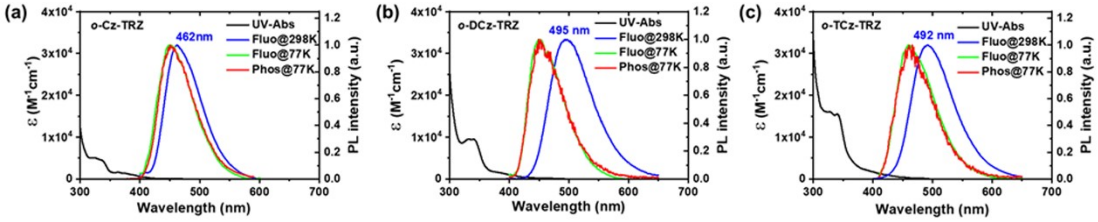

Fig. S5 UV-vis absorption, PL spectra of the investigated molecules measured in toluene solution (0.01 mM) in air at room temperature and low temperature fluorescence and phosphorescence measured in toluene solution (0.01 mM) in air at 77 K.

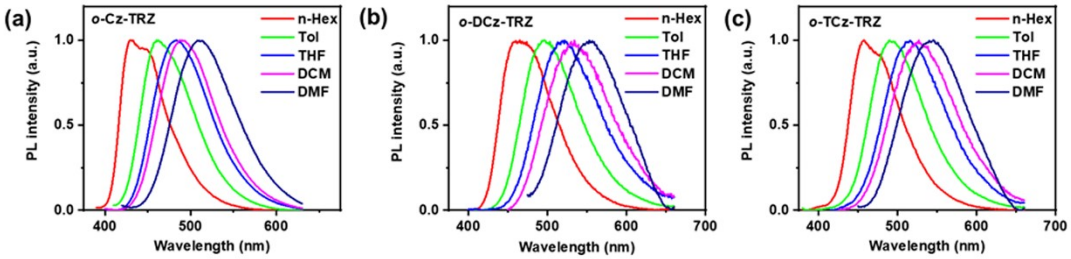

Fig. S6 PL spectra of the investigated molecules measured in different solvents (0.01 mM).

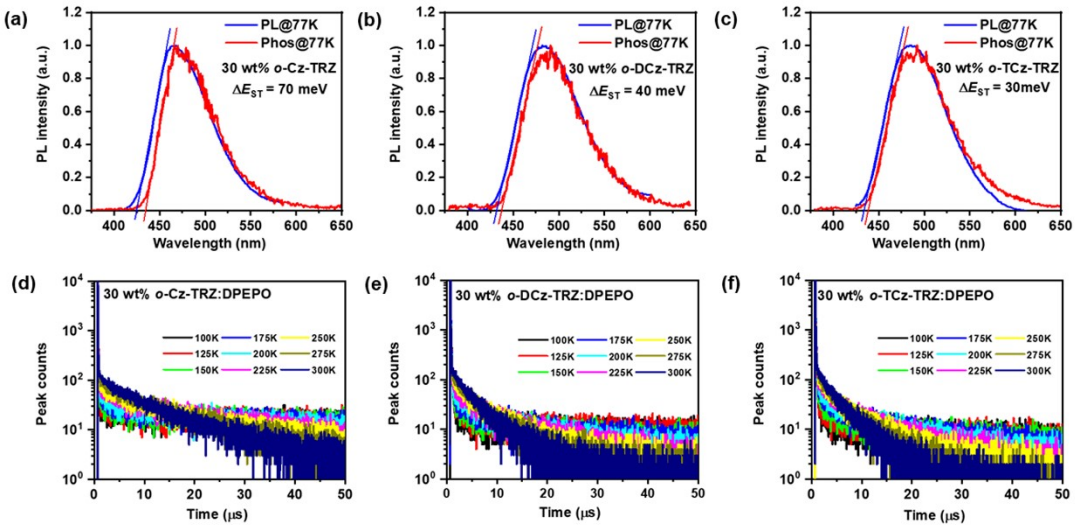

Fig. S7 (a-c) Low temperature fluorescence and phosphorescence spectra and (d-f) temperature-dependent transient PL decay curves (100 to 300 K) of *o*-Cz-TRZ, *o*-DCz-TRZ and *o*-TCz-TRZ doped into DPEPO films at the concentration of 30 wt%.

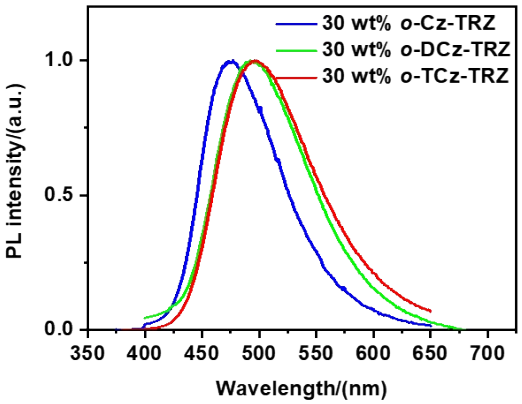

Fig. S8 PL spectra of the investigated molecules doped into DPEPO films at the concentration of 30 wt % measured under N_2 atmosphere at room temperature.

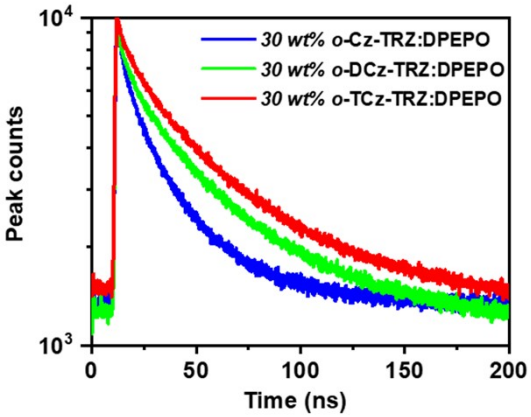

Fig. S9 Transient PL decay spectra of the investigated molecules doped into DPEPO films at the concentration of 30 wt % measured under N_2 atmosphere at room temperature.

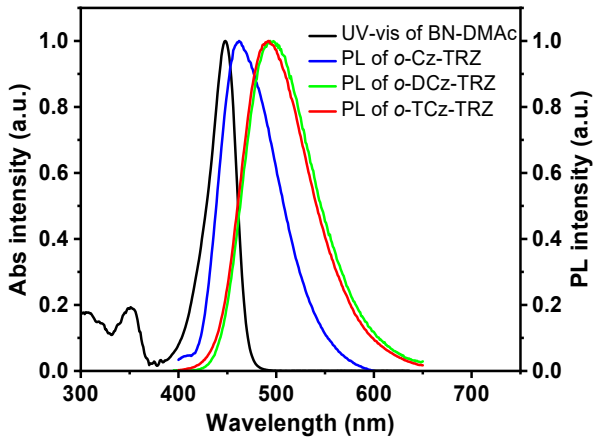

Fig. S10 UV-vis absorption spectrum of BN-DMAc and PL decay of the investigated molecules in dilute toluene solution.

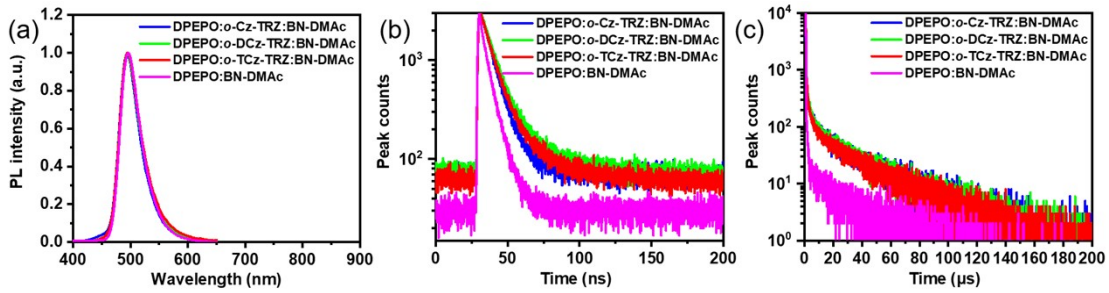

Fig. S11 PL spectra (a) and transient PL decay curves (c, d) of BN-DMAc doped into DPEPO with and without assistant hosts.

Table S1. Thermal, electrochemical and photophysical properties of the investigated molecules.

Compound	T_d[a]/T_g[b] (℃)	$HOMO$[c]/LUM (eV)	E_g[e] (eV)	$\lambda_{abs}\,sol$[f] (nm)	$\lambda_{PL}sol$[f]/$film$[g] (nm)	$S_1sol/film$[h] (eV)	$T_1sol/film$[h] (eV)	$\Delta E_{ST}\,sol/\Delta E_{ST}\,film$ (meV)
o-Cz-TRZ	375/62	-5.52/-2.89	2.63	360	460/475	3.03/2.92	3.02/2.85	10/70
o-DCz-TRZ	402/120	-5.38/-2.86	2.52	375	495/495	3.00/2.87	3.00/2.83	0/40
o-TCz-TRZ	515/165	-5.37/-2.85	2.52	380	492/498	2.98/2.85	2.98/2.82	0/30

[a] Decomposition temperature corresponding to a weight loss of 5 wt%. [b] Glass transition temperature. [c] Ionization potential (IP) measured by cyclic voltammetry. [d] Electron affinity (EA) calculated by IP minus optical gap approximated by the absorption edge in toluene (0.01 mM). [e] Energy gap estimated from the absorption edge in toluene (0.01 mM). [f] The longest peak wavelength of PL spectrum measured in

toluene (0.01 mM). [g] The peak wavelength of PL spectrum measured in DPEPO at the doping concentration of 30 wt%. [h] Energy levels of S_1 and T_1 estimated from the 0.01 mM toluene solution and 30 wt% doped film at 77 K.

Table S2. Photophysical properties of BN-DAMc (1 wt%) doped into DPEPO with and without assistant hosts.

Compound	PLQY (%)	ϕ_F (%)	ϕ_{TADF} (%)	ϕ_{ISC} (%)	τ_P (ns)	τ_{TADF} (μs)
DPEPO: BN-DMAc	52	45.7	14.3	54.3	5.89	15.51
DPEPO: *o*-Cz-TRZ: BN-DMAc	65	18.0	47.0	82.0	9.68	21.93
DPEPO: *o*-DCz-TRZ: BN-DMAc	69	13.7	55.3	86.3	13.0	21.85
DPEPO: *o*-TCz-TRZ: BN-DMAc	64	14.2	49.8	85.8	12.0	19.83

7. Device performance

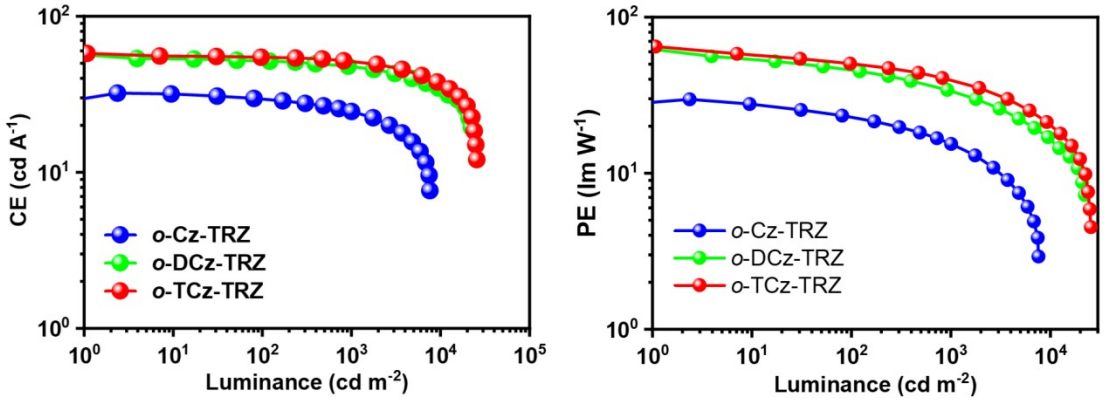

Fig. S12 Efficiency curves of the devices based on *o*-Cz-TRZ, *o*-DCz-TRZ and *o*-TCz-TRZ as the emitters.

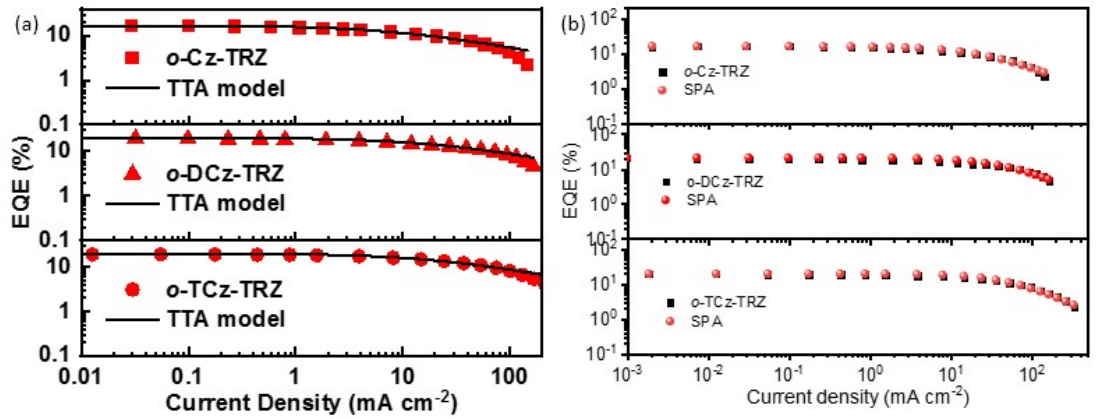

Fig. S13 Experimental EQE-current density characteristics and simulated efficiency roll-off curves based on TTA model (a) and singlet-polaron annihilation (SPA) model (b) of the devices based on *o*-Cz-TRZ, *o*-DCz-TRZ and *o*-TCz-TRZ as the emitters.

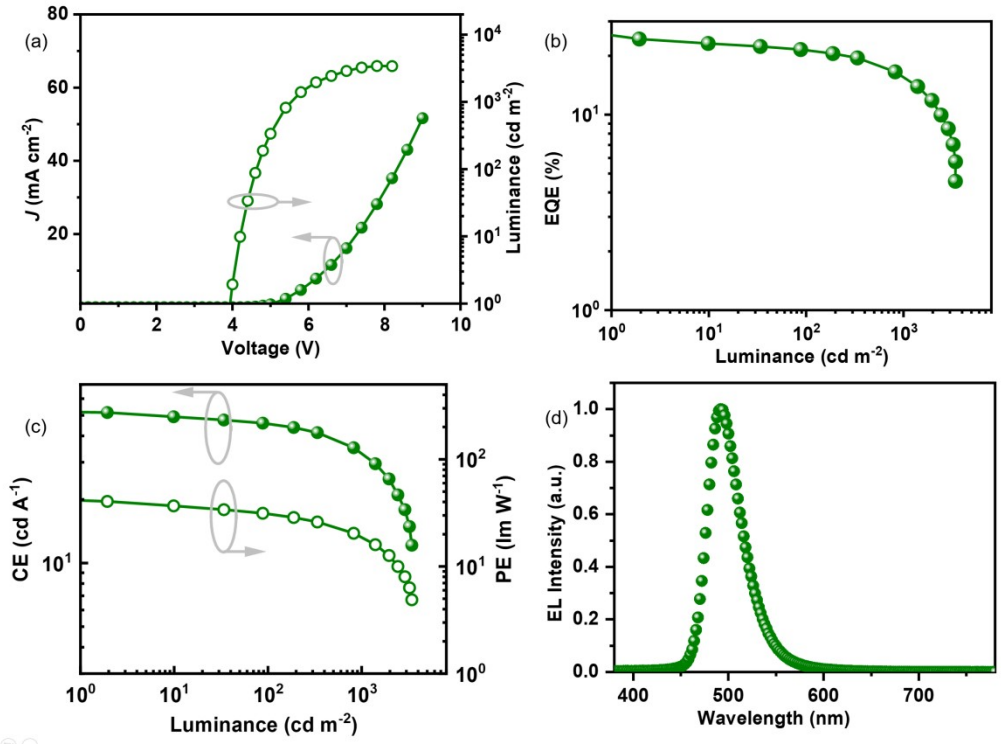

Fig. S14 *J-V-L* curves (a) efficiency curves (b and c) and EL spectrum (d) of the device based on BN-DMAc as the emitter and DPEPO as the host.

Table S3 EL performance of the devices based on the investigated molecules as the emitters at the doping concentration of 30 wt%.

EML	λ_{EL} (nm)	V_{on} (V)	Maximum			@ 100 cd m^{-2}		@ 1000 cd m^{-2}		CIE (x,y)
			EQE [%]	PE [lm W^{-1}]	CE [cd A^{-1}]	EQE [%]	CE [cd A^{-1}]	EQE [%]	CE [cd A^{-1}]	
o-Cz-TRZ	477	3.3	16.6	29.7	32.2	15.7	29.5	13.1	24.5	(0.16, 0.27)
o-DCz-TRZ	500	2.8	20.3	64.9	57.8	19.0	52.3	17.9	47.8	(0.23, 0.46)
o-TCz-TRZ	505	2.8	20.1	64.8	57.8	19.0	54.6	18.1	51.9	(0.24, 0.49)

Table S4. The key parameters of FRET processes.

Assistant hosts	R_0	k_{ET} (×10^8 s^{-1})	$Ø_{ET}$
o-Cz-TRZ	3.8	3.0	0.89
o-DCz-TRZ	4.6	8.8	0.96
o-TCz-TRZ	4.4	6.9	0.95

The rate of Förster energy transfer (FRET) from the donor to the acceptor k_{ET} is given by:

$$k_{ET} = \frac{1}{\tau_D}\left(\frac{R}{R_0}\right)^6 \quad \text{S2}$$

Where τ_D is the decay time of the donor in the absence of acceptor, R_0 is the Förster distance, and R is the donor-to-acceptor distance. The efficiency of FRET is given by

$$\emptyset_{ET} = \frac{k_{ET}}{k_{ET} + \frac{1}{\tau_D}} = \frac{1}{1 + \left(\frac{R}{R_0}\right)^6} \quad \text{S3}$$

Hence, the rate of energy transfer is equal to the decay rate of the donor (τ_D) when the D-to-A distance (R) is equal to R_0. The final equation of Förster energy transfer could be described as follows:

$$k_{ET} = \frac{9000(\ln 10)k^2\varphi_D}{128\pi^5 n^4 N_A \tau_D R^6} J_C \quad \text{S4}$$

where φ_D is the photoluminescence quantum yield (PLQY) of the donor in the absence of acceptor, n is the refractive index of the medium, N_A is Avogadro's number, J_C is the spectral overlap integral.

In an actual experiment it is usually easier to think about distances than energy transfer rates. For this reason, equation S4 could be written in terms of R_0 combining with equation 1 as follows:

$$R_0^6 = \frac{9000(\ln 10)k^2\varphi_D}{128\pi^5 n^4 N_A} J_C \quad \text{S5}$$

In this equation, k^2 is usually assumed to be 2/3 for a random distribution of donor-acceptor pairs, while n is about 1.7 for most of the organic materials.

Table S5 EL performance of the devices based on BN-DMAc as the terminal emitter with and without assistant hosts.

EML	λ_{EL} [nm]	V_{on} [V]	FWHM [nm]	L [cd m^{-2}]	$EQE_{max/100/1000}$ [%]	CE [cd A^{-1}]	PE [lm W^{-1}]	CIE [x,y]
DPEPO:*o*-Cz-TRZ:BN-DMAc	492	3.0	44	7358	22.7/19.4/14.9	48.9	51.2	(0.12, 0.40)

DPEPO:*o*-DCz-TRZ:BN-DMAc	496	2.9	46	11650	24.2/21.3/17.6	59.1	61.9	(0.13, 0.49)
DPEPO:*o*-TCz-TRZ:BN-DMAc	496	2.9	46	12650	23.9/21.5/17.9	61.7	66.0	(0.14, 0.49)
DPEPO: BN-DMAc	494	3.7	43	282.1	14.3/4.7/-	32.2	27.3	(0.11, 0.45)

Table S6 EL performance of the devices based on BN-DMAc as the terminal emitter using different hosts reported in the literatures.

Host	FWHM [nm]	$EQE_{max/100/1000}$ [%]	CE [cd A^{-1}]	references
DPEPO:*o*-Cz-TRZ	44	22.7/19.4/14.9	48.9	This work
DPEPO:*o*-DCz-TRZ	46	24.2/21.3/17.6	59.1	
DPEPO:*o*-TCz-TRZ	46	23.9/21.5/17.9	61.7	
mCBP	49	20.3/-/-	-	J. Mater. Chem. C, 2021, 9, 8308–8313
mCBP	48	21.1/19.7/12.5	55.2	Adv. Optical Mater., 2021, 9, 2100825
mCBP:PO-T2T	56	25.5/21.5/16.0	76.6	

8. References

1. D. Liu, D. Li, H. Meng, Y. Wang and L. Wu, Multifunctional applications of triazine/carbazole hybrid thermally activated delayed fluorescence emitters in organic light emitting diodes, *J. Mater. Chem. C*, 2019, **7**, 12470-12481.
2. J.-R. Cha, C. W. Lee, J. Y. Lee and M.-S. Gong, Design of ortho-linkage carbazole-triazine structure for high-efficiency blue thermally activated delayed fluorescent emitters, *Dyes Pigm.*, 2016, **134**, 562-568.
3. X. Cai, X. Li, G. Xie, Z. He, K. Gao, K. Liu, D. Chen, Y. Cao and S. J. Su, "Rate-limited effect" of reverse intersystem crossing process: the key for tuning thermally activated delayed fluorescence lifetime and efficiency roll-off of organic light emitting diodes, *Chem. Sci.*, 2016, **7**, 4264-4275.
4. W. Humphrey, A. Dalke and K. Schulten, VMD: Visual molecular dynamics, *J. Mol. Graph. Model.*, 1996, **14**, 33-38.
5. E. R. Johnson, S. Keinan, P. Mori-Sánchez, J. Contreras-García, A. J. Cohen and W. Yang, Revealing Noncovalent Interactions, *J. Am. Chem. Soc.*, 2010, **132**, 6498-6506.
6. T. Lu and F. Chen, Multiwfn: a multifunctional wavefunction analyzer, *J. Comput. Chem.*, 2012, **33**, 580-592.